scientific reports

Check for updates

OPEN

The marine xanthophyll diatoxanthin as ferroptosis inducer in MDAMB231 breast cancer cells

Clementina Sansone[1]✉, Luigi Pistelli[1,2] & Christophe Brunet[1]

Marine biotopes are considered as a huge reservoir of biodiversity and chemodiversity, the latter potentially providing new treats for health prevention. Among the emphasized marine biocenosis, microorganisms such as microalgae propose suitable solutions to address eco-sustainability or biorefinery topics. The health interests of the xanthophyll diatoxanthin (Dt), a photoprotective and antioxidant pigment synthetized by diatoms, have been recently documented. This study deeply explores the capacity of Dt to intercept cancer progression and addresses the Dt -induced cell death in breast cancer. It is crucial to know which signalling pathway explaining its function is induced by the molecule in the targeted cells. This study disentangled the intracellular effects of Dt in MDAMB231 breast cancer cells. The results highlighted the inhibition of glutathione synthesis through cysteine transport blockage, that in turn, induced an iron accumulation and increase in lipid peroxidation. Those features represent the principal hallmarks of intracellular ferroptosis pathway. Ferroptosis being considered as one of the cell death most promising in fighting cancer development (e.g. in breast cancer) this study reinforces the scientific/biomedical interests on Dt and the diatoms' resource and paves the way to explore its suitability in vivo.

Keywords Xanthophyll, Diatoms, Ferroptosis, Oxidative stress-induced cell death, Ferrostatin, Erastin

Breast cancer (BC) is one of the most leading causes of woman death in developed countries[1]. The less sensitive form of BC to conventional chemotherapeutic agents is represented by the triple-negative breast cancer (TNBC), with a high malignancy index in terms of metastasis formation due to its triple-negative status for the progesterone receptor, the estrogen receptor, and human epidermal growth factor receptor-2[2]. TNBC represents the 10–15% of breast cancers, and its mortality rate amounts to 40% within the first five years after diagnosis[2]. The weak effect of conventional chemotherapeutic practices on this cancer leads to consider other therapeutic approaches, than radiotherapy, chemotherapy, or surgery.

Ferroptosis is a recently discovered essential type of intracellular iron-dependent form of regulated cell death (RCD) characterized by iron overload and lipid peroxidation with unclear molecular mechanisms[3] and different from apoptosis, necrosis, and autophagy[4]. Ferroptosis can be triggered through either extrinsic or intrinsic pathway. The extrinsic pathway initiates through the regulation of transporters (e.g. inhibition of the amino acid antiporter system termed xc^- or activation of the iron transporters transferrin and lactotransferrin), whereas the intrinsic pathway is mainly induced by blocking the expression or activity of intracellular antioxidant enzymes, such as Phospholipid hydroperoxide glutathione peroxidase 4 (GPX4)[5]. Previous evidence defined ferroptosis as "the achilles' heel" of breast cancer for its unique metabolism, high levels of reactive oxygen species (ROS), and related gene mutations[6]. Ferroptosis susceptibility of BC is attributed to several metabolic characteristics, including high polyunsaturated fatty acids (PUFAs) levels, expanded liable iron pool, and weakened GPX4-glutathione (GSH) defense system[7]. On the other hand, the innate accumulation of iron in BC determines a huge amount of ROS, due to the interaction of ferrous iron ion and hydrogen peroxide in cells. Accumulated intracellular ROS start to react with PUFAs, causing lipid peroxidation and ultimately leading to ferroptosis. For this reason, patients with breast cancer exhibit serum levels of form of iron sixfold higher than the normal population[8]. At molecular level, Transferrin (TF), Transferrin Receptor (TFRC) and Solute Carrier Family 11 Member 2 (SLC11A2), which are responsible for importing iron into cells, are also expressed at higher levels in breast carcinoma than normal tissues, while the iron exporter Solute Carrier Family 4 Member 1 (SLC4A1) exhibited lower expression levels[9]. It was demonstrated that the expression of TFRC regulated intracellular total iron and proliferation and invasion of the breast cancer cells, both in vitro and in vivo[10].

[1]Stazione Zoologica Anton Dohrn, sede Molosiglio, via F. Acton, 80133 Naples, Italy. [2]Clinical and Experimental Unit of Breast Cancer, National Cancer Institute, IRCCS "Fondazione G. Pascale", Naples, Italy. ✉email: clementina.sansone@szn.it

Numerous studies have demonstrated the potential relevance of ferroptosis in inhibiting tumor growth[3,6], as well as the role of some natural phytochemicals in regulating this mechanism in breast cancer cells[10,11]. It is noteworthy the necessity to further enrich our understanding of the various natural product-mediated mechanisms regulating ferroptosis and expand our knowledge of the regulatory mechanisms involving ferroptosis-related signaling pathways and associated metabolic pathways[11]. In the natural reservoir of bioactive molecules, marine compounds are of great interest. For instance, marine carotenoids, taxanes, or flavonoids, can be used as anticancer agents, also offering strategies to overcome chemoresistance and present anti-inflammatory, anti-proliferative, anti-angiogenic, and antioxidant properties[12]. To date, there are no evidence of marine natural compounds provided with a function of ferroptosis inducer.

The microalgae from the group of diatoms contain the xanthophyll diatoxanthin (Dt), which quickly and efficiently protects cells from light induced oxidative damages[13,14] and modulates intracellular iron metabolism and concentration[15]. Recently, Dt showed chemopreventive and angiopreventive effects in MDAMB231 cancer cells by inhibiting spheroids formation and by downregulating genes involved in inflammation and tumorigenic pathways[16].

The present study explores the chemopreventive function of Dt in MDAMB231 cancer cells[17], exploring the signaling pathway involved in the Dt-induced cell death. The aim is to further enrich the understanding of the marine natural product-mediated mechanisms regulating ferroptosis-like pathways and expand our knowledge of the regulatory in vitro mechanisms involving ferroptosis-related signalling pathways and associated metabolic pathways. This study demonstrates that the Dt-induced MDAMB231 cell death occurs by (i) targeting GPX4 gene and protein expression, (ii) inducing peroxidation of the high PUFAs and (iii) by affecting the expression of TF, TFRC and SLC11A2 genes, which are responsible for intracellular iron intake. Our results propose Dt as a ferroptosis-like pathway inducer and pave the way to further explore its efficiency in vivo aiming to take into account the use of this xanthophyll for breast cancer prevention and therapy.

Results

Dt inhibits triple negative breast cancer cell viability

Diatoxanthin (Dt) significantly inhibited the growth of MDAMB231 and MDAMB468 cells ($p \leq 0.0001$), while no effect was reported on the three no-malign cell lines (i.e., human dermal fibroblasts, melanocytes and HaCat, Fig. 1). The 50% of growth inhibition of Dt in MDAMB231 cells was $IC_{50} = 6$ ng $ml^{-1} \pm 0.7$, which is a very low concentration also compared to the other MDAMB468 cell line in which $IC_{50} = 15$ ng $ml^{-1} \pm 1.25$. Therefore, MDAMB231 cell line was selected for the following experiments to more in deep investigate the mechanism of action at molecular level.

Dt modulates ferroptosis-related protein expression in MDAMB231 cells

Proteins involved in glutathione and iron metabolism are key targets in the ferroptosis mechanism[18]. The transferrin receptor (TFRC), required for transferrin-iron complex uptake into cells, was significantly over expressed in MDAMB231 cells treated with Dt ($p < 0.0001$, Fig. 2) compared to untreated cells. Also, the ferritin heavy chain (FHC), a protein involved in the iron ion storage, was significantly overexpressed in presence

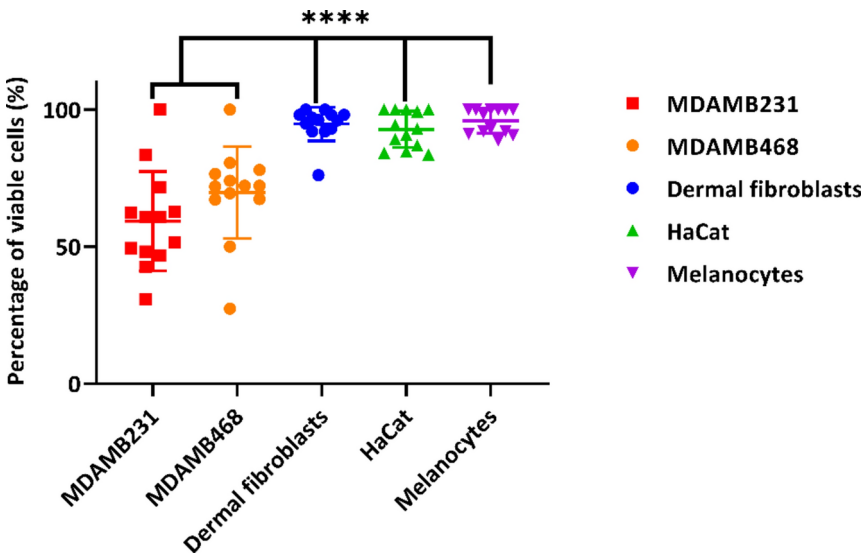

Fig. 1. Effect of Dt on the viability of five cell lines: the two cancer lines MDAMB231 and MDAMB468, and the three normal cell lines (Dermal fibroblasts, HaCat and Melanocytes). Experiments were carried out in triplicate with twelve Dt concentrations: 0.1, 0.5, 1, 1.5, 2, 2.5, 5, 7.5, 10, 12.5, 15 and 25 ng mL^{-1}. Values represent means ($n = 3$) with respective standard deviations. Asterisks indicate the statistically significant difference compared to the normal cell lines used as respective controls (**** $p \leq 0.0001$; Dunnett's multiple comparisons test).

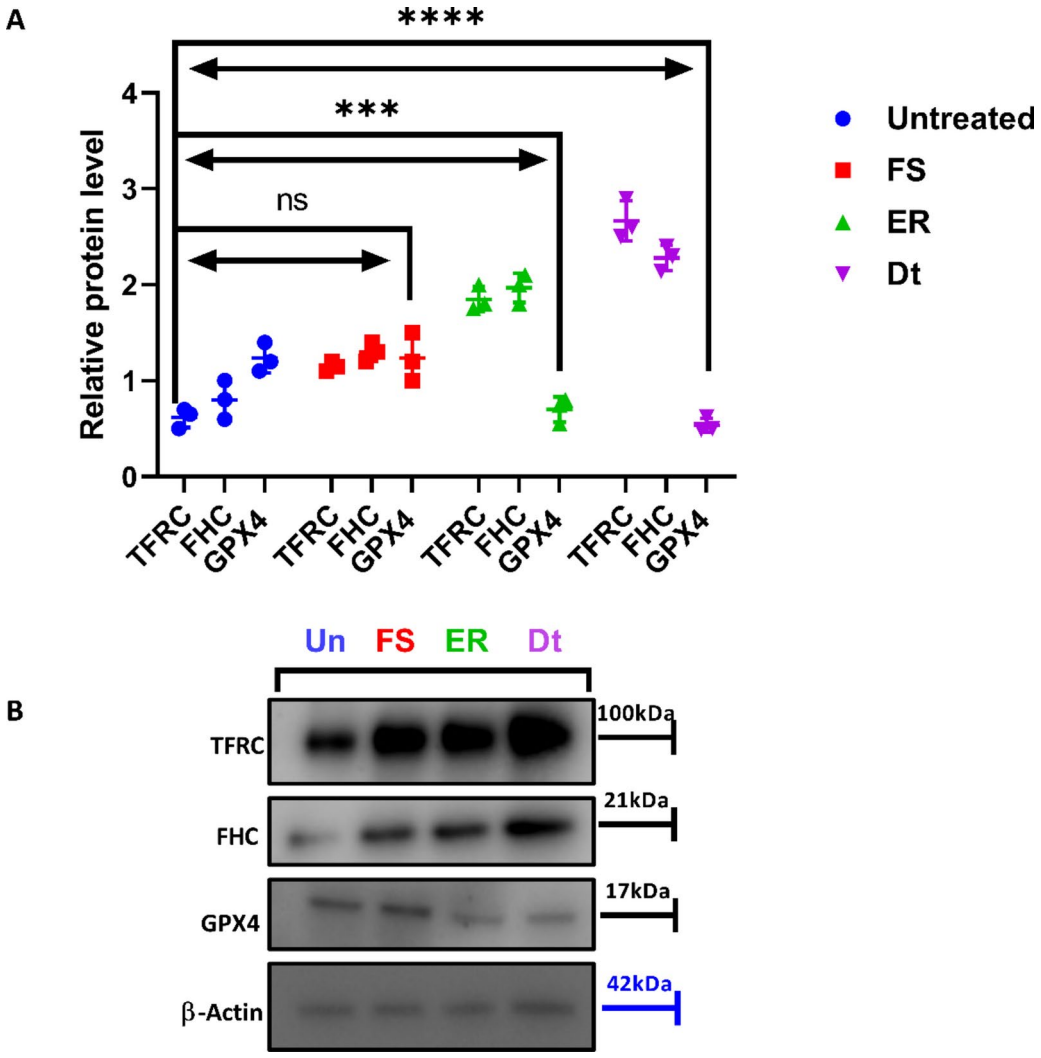

Fig. 2. (**A**) Expression of the three proteins transferrin receptor (TFRC), ferritin heavy chain (FHC), and glutathione peroxidase 4 (GPX4), through western blot analysis) after 24 h of incubation of MDAMB231 cells with Dt (at IC_{50} dose of 6 ng ml^{-1}), FS (60 nM), or ER (10 μM). Results were normalized to β-Actin. The values represent the mean ± SEM (n = 3). Asterisks indicate the statistically significant difference compared to the untreated cells (***$p < 0.001$, ****$p < 0.0001$; Dunnett's multiple comparisons test). (**B**) Representative immunoblot analyses of MDAMB231 cells after 48 h of treatment with FS (60 nM), ER (10 μM) or Dt (6 ng mL^{-1}).

of Dt ($p < 0.0001$, Fig. 2). Conversely, the lipid repair enzyme glutathione peroxidase 4 (GPX4) was strongly down-expressed in presence of Dt ($p < 0.0001$, Fig. 2). In presence of erastin (ER), TFRC and FHC were also overexpressed, while GPX4 was down-expressed compared to the control (untreated cells; $p < 0.001$, Fig. 2). Finally, ferrostatin (FS) did not induce any change of expression of those proteins compared to untreated cells ($p > 0.05$).

Dt triggers intracellular Fe^{2+} levels increase in MDAMB231 cells

The Dt-related overexpression of ferritin is probably linked to an increase of intracellular Fe^{2+} storage, which was revealed in MDAMB231 cells in presence of Dt (6 ng ml^{-1}, Fig. 3B) compared to the control (untreated cells, Fig. 3A).

Dt affects glutathione metabolism in MDAMB231 cells

Following the down-expression of GPX4 protein, Dt induced a significant decrease of reduced glutathione (GSH) in MDAMB231 cells compared to the untreated cells ($p < 0.01$, Fig. 4). Conversely, the intracellular concentration of oxidized glutathione (GSSG) was not affected by Dt, showing similar levels both in treated and untreated cells (Fig. 4).

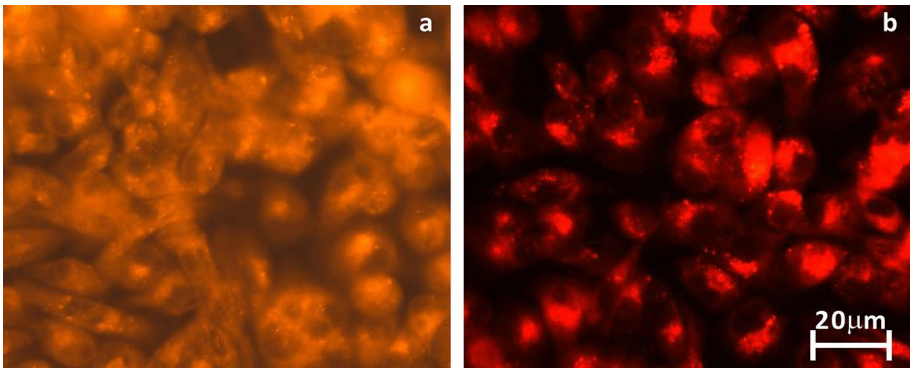

Fig. 3. Epifluorescence pictures (using FerroOrange dye) of iron accumulation in untreated MDAMB231 cells (**A**) and Dt-treated MDAMB231 cells (Dt 6 ng ml^{-1}) (**B**). This assay revealed the relative intracellular Fe^{2+} level (scale bar: 20 µm).

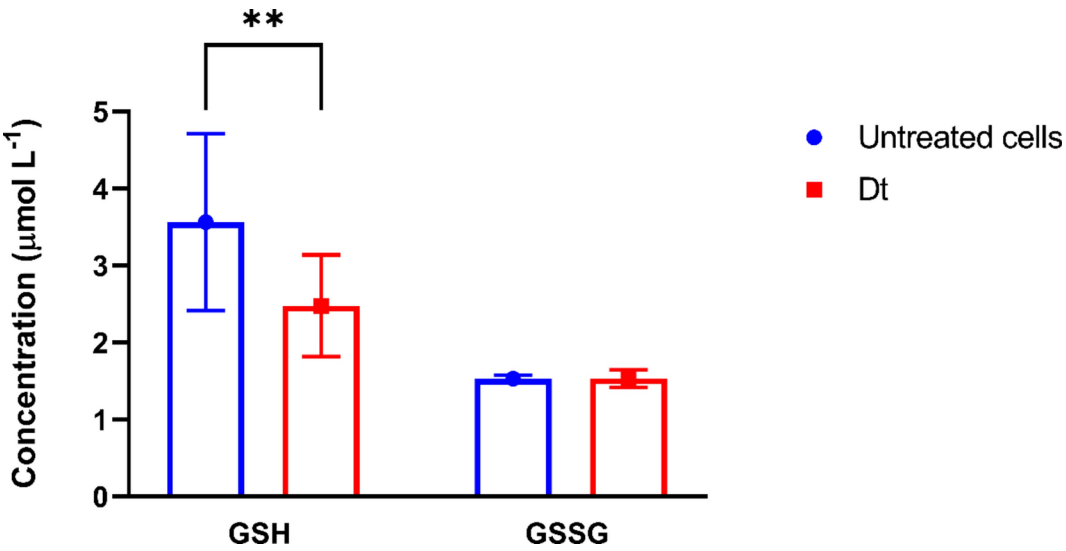

Fig. 4. Concentration of reduced glutathione (GSH) and oxidized glutathione (GSSG) in MDAMB231 cells after 24 h of incubation in absence or presence of Dt (6 ng ml^{-1}). Values represent means (n = 3) with respective standard deviations. Asterisks indicate the statistically significant difference compared to the untreated cells (** $p < 0.01$; Sidak's multiple comparison test).

Dt induces lipid peroxidation in MDAMB231 cells

The decrease of GSH, the overexpression of the TFRC protein and the increase in intracellular Fe^{2+} led to lipid peroxidation (Fig. 5). After 24 h of incubation, the induction of lipid peroxidation by Dt was significantly higher than all the other treatments, also compared with that exerted by the ferroptosis-inducer ER ($p < 0.0001$; Fig. 5A,B). FS stably prevented lipid peroxidation ($p > 0.05$; Fig. 5A, B-III), while the addition of Dt together with FS induced a lipid peroxidation increase ($p < 0.0001$; Fig. 5A,B-V).

At shorter incubation times (1 or 3 h), the effects of Dt on lipid peroxidation were still significant compared to untreated cells or FR-treated cells ($p < 0.0001$; Fig. 5A) and similar to the effect of ER, ER + FS or FS + Dt ($p < 0.0001$, Fig. 5A).

Dt modulates ferroptosis-related gene expression in MDAMB231 cells

The activation of the ferroptosis pathway activation was assessed at molecular level by targeting key genes expression involved in ferroptosis at 1, 3 and 24 h of treatment (Tables S1, S2, S3 and S4). A selection of genes related to signal transduction pathway previously presented at protein and phenotypic levels was done with macrofamilies genes involved in ferroptosis activation (red and violet groups) and key factors implicated in glutathione synthesis and modulation, e.g. Glutathione Synthetase (GSS) and Glutathione Peroxidases (GPXs), in iron metabolism and storage, e.g. TFRC, Ferritin Light Chain (FTL) and Ferritin Heavy Chain 1 (FTH1), and in autophagy (brown group) (Fig. 6).

The expression of the gene Solute Carrier Family 7 Member 11 (SLC7A11, xCT, red group, Fig. 6 and Table S2, S3 and S4), a subunit of system xc^-, was significantly downregulated with Dt (-12.57, -4.48 and -13.38 in

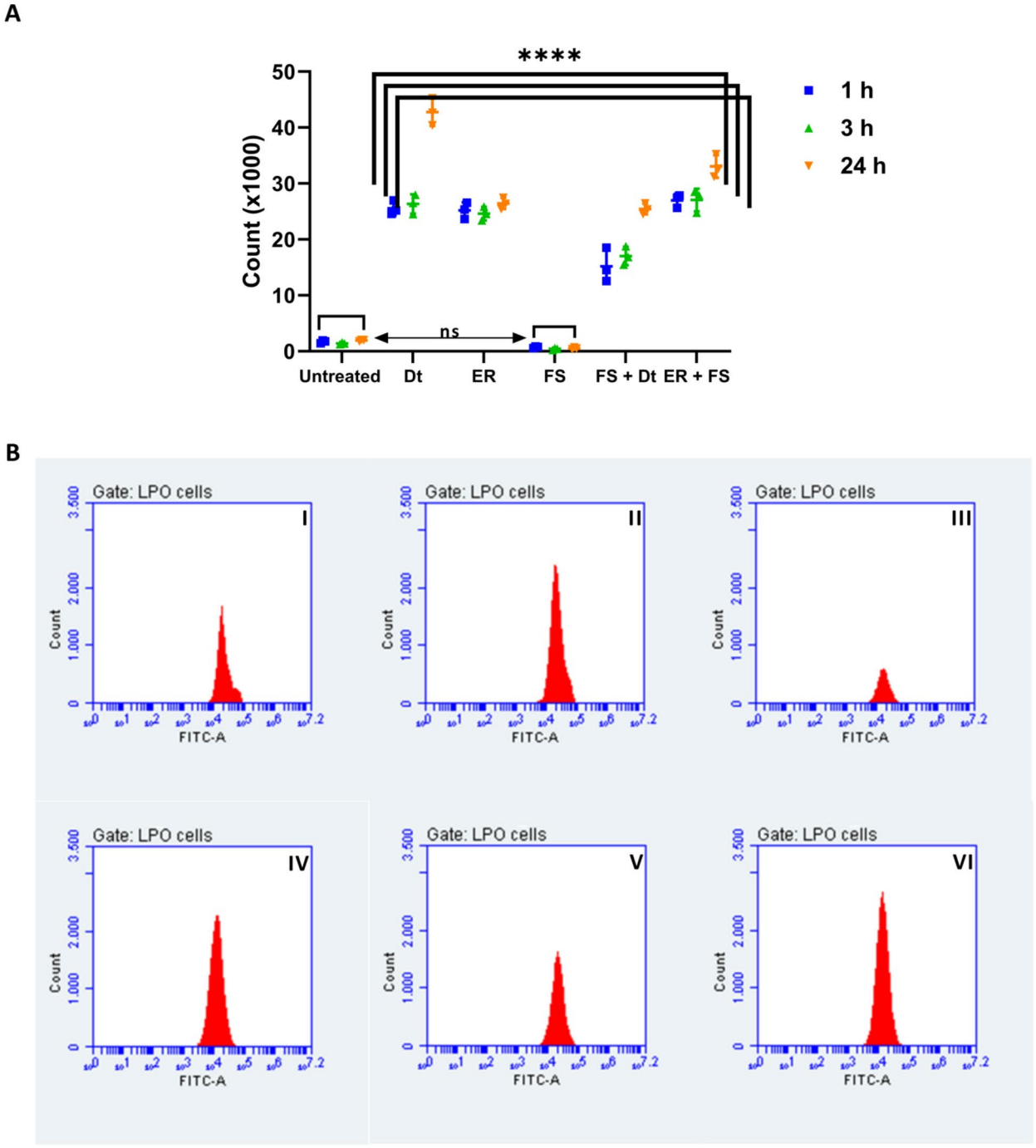

Fig. 5. (**A**) Relative levels of cells showing lipid peroxidation in MDAMB231 cells after 1, 3 or 24 h of incubation with Dt (6 ng ml^{-1}), FS (60 nM), ER (10 µM), FS + Dt (60 nM and 6 ng ml^{-1}, respectively) or ER + FS (10 µM and 60 nM, respectively). Values represent means (n = 3) with respective standard deviations. Asterisks indicate the statistically significant difference compared to the untreated cells (****$p < 0.0001$; Dunnett's multiple comparisons test). (**B**) Cytograms of the fluorescence index by FITC-A correlated to the cell number i.e., the number of lipid peroxidation (LPO) positive cells: untreated (**I**), Dt (**II**), FS (**III**), ER (**IV**), FS + Dt (**V**) and ER + FS (**VI**) for 24 h. Cells positive in FITC-A channel are directly proportional to the lipoxidation level of cell membranes.

fold regulation at 1, 3 and 24 h, respectively). Treatment with ER upregulated SLC7A11 expression at 1 and 24 h (15.65 and 34.00 in fold regulation, respectively), as it occurred with FS after 1 and 24 h (37.50 and 24.80 in fold regulation, respectively), while SLC7A11 expression was slightly downregulated at 3 h (-5.76 in fold regulation). Combination of FS and Dt induced an expression downregulation of SLC7A11 (-37.50, -6.00 and -24.80 in fold regulation at the three times, respectively), while the combination of ER and FS downregulated the expression of

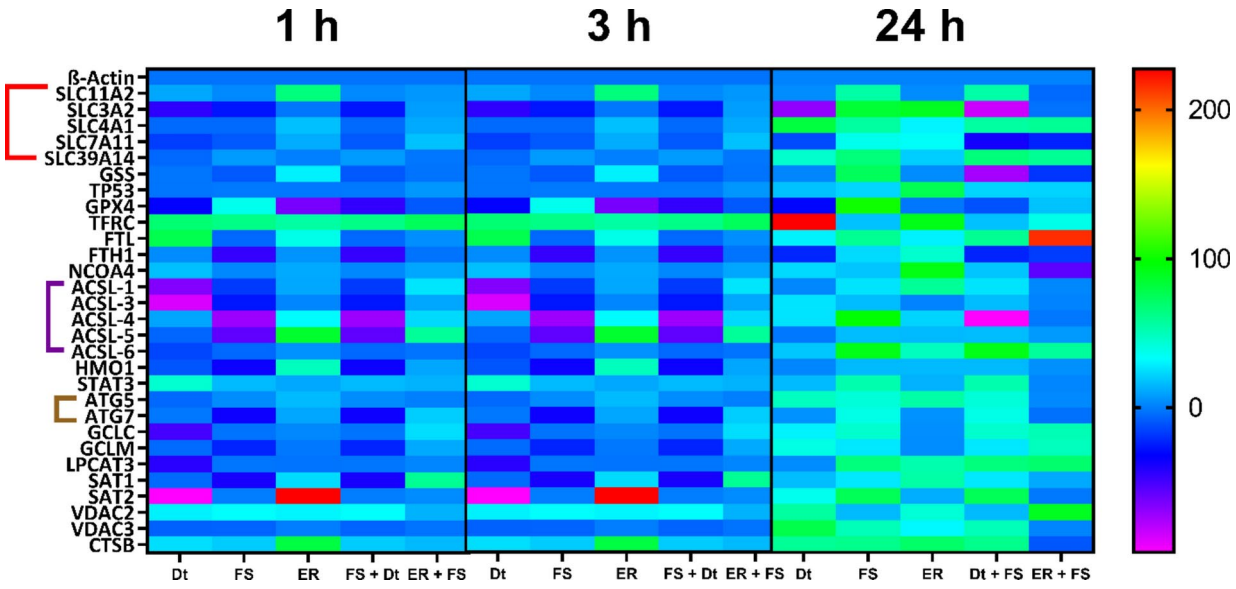

Fig. 6. RT-PCR analysis of ferroptosis-involved genes with cDNA microarrays in MDAMB231 cells treated with Dt (6 ng ml^{-1}), FS (60 nM), ER (10 µM), FS + Dt (60 nM and 6 ng ml^{-1}, respectively) and ER + FS (10 µM and 60 nM, respectively). The experimental time course was represented by incubation time of 1, 3 and 24 h. The heatmaps indicated the mRNA expression level of ferroptosis-involved genes (Z-score). Specific gene families: cell membrane harbors system xc^- (red group), long-chain acyl-CoA synthetase family (violet group) and autophagy (brown group).

SLC7A11 after 1 and 24 h of treatment (-23.86 and -21.79 in fold regulation, respectively) with an upregulation of its expression after 3 h (21.00 in fold regulation).

Dt was able to upregulate the expression of the Acyl-CoA Synthetase Long Chain Family Member 4 (ACSL-4, 13.72, 4.43 and 25.37 in fold regulation at 1, 3 and 24 h, respectively, Fig. 6 and Tables S2, S3 and S4). ACSL-4 expression was also upregulated with ER treatment (35.46, 53 and 22.00 in fold regulation at 1, 3 and 24 h, respectively). The treatment with FS induced a downregulation of the ACSL-4 gene after 1 h of incubation (-67.95 in fold regulation), while it upregulated ACSL-4 gene expression at longer incubation (93.66 and 97.11 in fold regulation at 3 and 24 h, respectively). Combination of FS and Dt induced a downregulation of ACSL-4 (-67.95, -93.66 and -97.11 in fold regulation at the three times, respectively). By contrast, combination of ER and FS induced an upregulation of ACSL-4 after 1 and 3 h of treatment (27.00 and 15.82 in fold regulation, respectively) and no change in ACSL-4 expression after 24 h (-1.86 in fold regulation).

The expression of the gene Solute Carrier Family 3 Member 2 (SLC3A2) involved in the transporter system xc^- was downregulated by Dt (-40.01, -31.81 and -69.55 in fold regulation at the three times, respectively, Fig. 6 and Tables S2, S3 and S4). On the contrary, ER induced an upregulation of SLC3A2 expression (4.03, 23.00 and 89.00 in fold regulation at the three times, respectively). Treatment with FS firstly induced a downregulation of the SLC3A2 gene (-22.75 in fold regulation at 1 h) while upregulated it later (17.63 and 84.27 in fold regulation at 3 and 24 h, respectively, Fig. 6 and Tables S2, S3 and S4). Combination of ER and FS induced the same effect than ER i.e., an upregulation of SLC3A2 (7.92 in fold regulation at 1 h) followed by a downregulation (-70.28 and -3.33 in fold regulation at 3 and 24 h, respectively). Combination of FS and Dt downregulated SLC3A2 expression (-22.75, -17.63 and -84.27 in fold regulation at the three times, respectively, Fig. 6 and Tables S2, S3 and S4).

GSS expression was upregulated with ER (32.66, 13.00, and 3.00 in fold regulation at 1, 3 and 24 h, respectively; Fig. 6 and Tables S2, S3 and S4), and with FS at 3 and 24 h (22.00 and 74.24 in fold regulation, respectively), while it was downregulated with FS after the shorter incubation (-5.89 in fold regulation at 1 h). Dt did not induce any expression variation after 1 or 24 h (1.64 and 1.68 in fold regulation, respectively), Dt downregulated this gene expression after 3 h of incubation (-20.00 in fold regulation). Combination of FS and Dt downregulated GSS expression (-5.89, -22.00 and -74.24 in fold regulation at the three times, respectively), while ER + FS significantly downregulated GSS expression after 3 and 24 h of treatment (-9.96 and -19.00 in fold regulation, respectively), without any gene expression modulation at shorter incubation (1.00 in fold regulation at 1 h, Fig. 6 and Tables S2, S3 and S4).

Downregulation of GPX4 was observed with Dt treatment (-28.72, -20.17 and -31.1 in fold regulation at 1, 3 and 24 h, respectively), and ER treatment (-58.37, -40.00 and -2.00 in fold regulation at 1, 3 and 24 h, respectively; Fig. 6 and Tables S2, S3 and S4). Conversely, incubation of cells with FS induced an up-regulation of the GPX4 gene (40.44, 94.20 and 101.68 in fold regulation at 1, 3 and 24 h, respectively). The combination of FS and Dt induced a downregulation of GPX4 (-40.44, -14.20 and -11.68 in fold regulation at the three times, respectively), while ER and FS together induced a slight downregulation of GPX4 after 1 and 3 h of treatment

(-6.00 and -3.03 in fold regulation, respectively) with an upregulation at 24 h (17.26 in fold regulation, Fig. 6 and Tables S2, S3 and S4).

The Nuclear Receptor Coactivator 4 (NCOA4) gene expression was firstly upregulated by Dt after 1 h (20.40 in fold regulation) and then downregulated (-78.28 and -2.90 in fold regulation at 3 and 24 h, respectively, Fig. 6 and Tables S2, S3 and S4). ER induced a constant upregulation of NCOA4 (14.95, 11.00 and 93.00 in fold regulation at the three times, respectively). The same was found with FS (6.44, 7.06 and 18.00 in fold regulation at the three times, respectively). The combination of FS and Dt upregulated NCOA4 expression after 1 and 24 h (6.44 and 18.00 in fold regulation, respectively) while a downregulation as reported at 3 h (-78.28 in fold regulation, Fig. 6 and Tables S2, S3 and S4). Conversely, the combination of ER and FS firstly upregulated NCOA4 expression (14.00 and 33.33 in fold regulation at 1 and 3 h, respectively) and then downregulated it (-56.00 in fold regulation at 24 h, Fig. 6 and Tables S2, S3 and S4).

TFRC (blue group) gene expression was upregulated with Dt (72.00, 155.00 and 227.43 in fold regulation at 1, 3 and 24 h, respectively), with ER (59.03, 62.00 and 92.00 in fold regulation at 1, 3 and 24 h, respectively) or with FS (66.74, 21.30 and 16.97 in fold regulation at 1, 3 and 24 h, respectively, Fig. 6 and Tables S2, S3 and S4). Although the combination of ER and FS induced an upregulation of TFRC (78.00, 49.21 and 37.81 in fold regulation at 1, 3 and 24 h, respectively, Fig. 6 and Tables S2, S3 and S4), the contemporary addition of FS and Dt upregulated TFRC expression at 1 and 24 h (66.74 and 16.97 in fold regulation, respectively), but inducing its downregulation at 3 h of treatment (-21.30 in fold regulation, Fig. 6, and Tables S2, S3 and S4).

Autophagy Related 5 (ATG5) gene was strongly upregulated by Dt after 3 and 24 h of treatment (92.41 and 48.48 in fold regulation respectively) while Autophagy Related 7 (ATG7) gene was slightly upregulated by Dt after 1 and 24 h of treatment (2.11 and 4.98 in fold regulation, respectively) (Fig. 6 and Tables S2, S3 and S4). Autophagy Related genes are affected also by ER and FS treatment, due to the intracellular autophagy pathway activation for the nutritional homeostatic intake.

In vitro stability of Dt

Results from HPLC analysis revealed that Dt was still detected after 1 h in human plasma (20% of T0; Fig. 7), suggesting a suitable stability of Dt. The Dt half-life ($t_{1/2}$) was estimated ≈ 25 min.

In the culture medium or simulated body fluid (SBF) (Figure S2) Dt was still present after 24 h (≈ 30% compared to T0). Conversely, with the presence of MDAMB231 cells in the medium, Dt significantly decreased after 1 h, almost disappearing at 3 h (Figure S2).

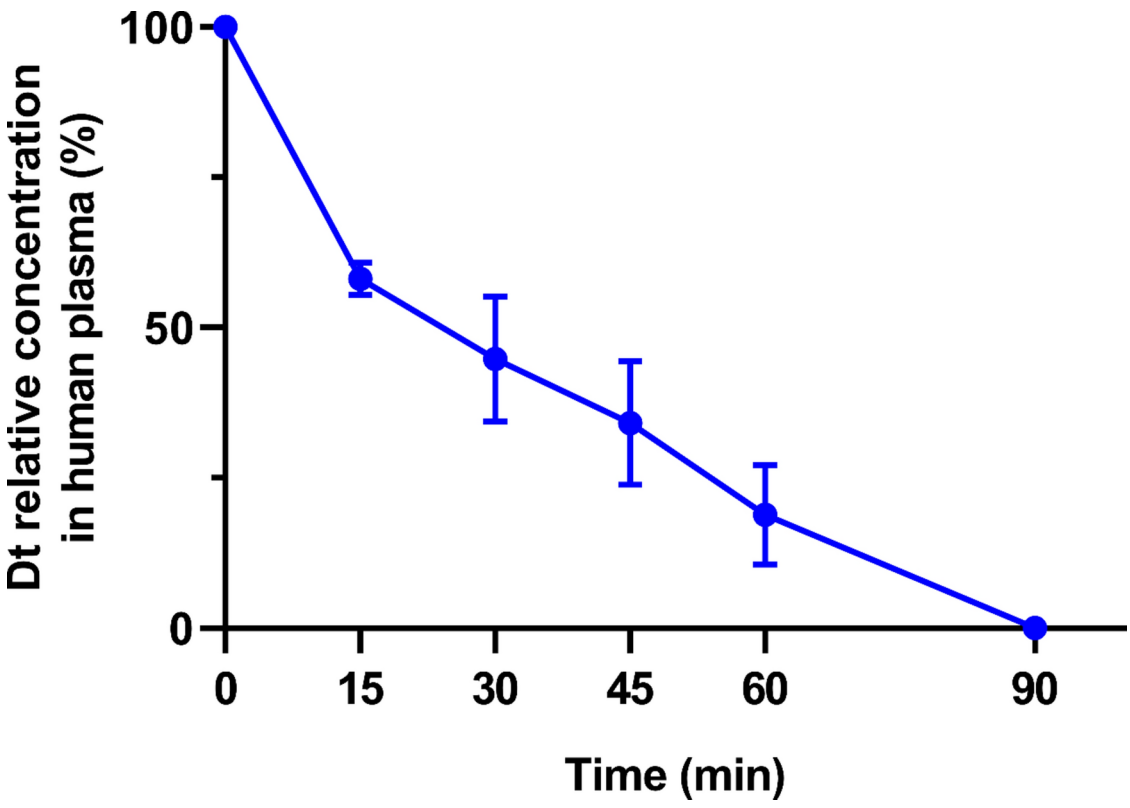

Fig. 7. Time decreasing rate of Dt in vitro in human plasma (sampling at 0, 15, 30, 45, 60 and 90 min). Axis Y: percent of Dt as relative concentration measured at each sampling time *vs* time T0. Values represent means (n = 3) with respective standard deviations. The in vitro plasma half-life ($t_{1/2}$) of Dt was estimated at 25 min (see text).

Discussion

Ferroptosis is a regulated cell death (RCD) mechanism driven by intracellular iron increase and resulting in oxidative stress, reactive oxygen species (ROS) generation and lipid peroxide (Lipid-OOH) accumulation[19]. This RCD plays a crucial role in cancer therapy, especially in cancer cells sensitive to oxidative stress and intracellular iron accumulation[20]. Breast cancer might be one of the targets in which ferroptosis appears to be a promising cell death mechanism for cancer interception[21].

Investigation on ferroptosis-inducer compounds—to be applied both alone or in combination with chemotherapeutics—is therefore a relevant topic[18,21]. Current preclinical experiments suggest that several classes of phytochemical compounds, such as flavonoids, alkaloids, phenols, lignans and saponins, have shown the potential to induce ferroptosis in breast cancer[9]. For instance, the phytochemical dihydroartemisin induces ferroptosis in liver cancer cells by reducing glutathione (GSH) content, downregulating phospholipid hydroperoxide glutathione peroxidase (GPX4) protein levels and increasing ROS levels[22]. In the triple negative breast cancer (TNBC) cells, the deficiency of cysteine is a feature that make these cells highly sensitive to ferroptosis[23]. In TNBC ferroptosis is triggered by the natural product glycyrrhetinic acid, which promotes the generation of ROS and reactive nitrogen species (RNS) by activating NADPH oxidase and inducible nitric oxide synthase (iNOS)[24]. This leads to the reduced activity of GSH and GPX, increasing lipid peroxidation, and initiating ferroptosis[24]. Yet, the sesquiterpene lactone eupaformosanin was shown to induce apoptosis and ferroptosis by targeting the ubiquitination of GPX4 in TNBC[24]. In an another breast cancer cell line, MDAMB231, the mechanism of ferroptosis induced by erastin (ER) is even enhanced by the combination of ER with holo-lactoferrin i.e., iron-saturated form of lactoferrin[25].

While marine biodiversity is considered as a reservoir of bioactive secondary metabolites, marine-originated compounds are still not known as ferroptosis-inducer molecules. Carotenoids represent a class of highly active and diverse compounds, with some of them exclusively aquatic[26]. This study focusses on one of them, the diatoxanthin (Dt)[26,27]. Dt is prone to fight several biological processes involved in inflammation and tumor development and metastasis, as demonstrated by RNA-Seq data[16]. Previous studies reported that Dt in combination with the chemotherapeutic agent doxorubicin inhibits TNBC spheroid growth, reducing their 3D-integrity and decreasing the viability of MDAMB231 cells[16].

This study reveals that MDAMB231 cells treated with Dt report all the hallmarks typical for ferroptosis[10], as also confirmed by the comparative analysis using ferroptosis inhibitor ferrostatin-1 (FS) or ferroptosis activator ER. Dt inhibits the cell membrane harbors system xc^-, composed primarily of solute carrier family 3 member 2 (SLC3A2) and solute carrier family 7 member 11 (SLC7A11), with consequential decrease in GSH synthesis, leading to the accumulation of superoxide and triggering ferroptosis. Dt upregulates the expression of tumor suppressor, the tumor protein P53 (TP53) which is known to inhibit system xc^- and cause ferroptosis by downregulating SLC7A11[28]. It is noteworthy that TP53 downregulates SLC7A11, disrupts cystine uptake by system xc^-, interferes with GSH synthesis and induces ferroptosis[29]. The functional enzyme GPX4 mitigates lipid peroxidation by utilizing GSH, and the inhibition of GPX4 activity – as reported in this study for Dt—triggers phospholipid peroxidation and induction of ferroptosis[30]. The inhibition of GPX4 leads to the accumulation of polyunsaturated fatty acids (PUFAs) and ROS, resulting in plasma membrane damage and subsequent ferroptosis[20]. The essential enzymes that participate in the lipid peroxidation are the long-chain acyl-CoA synthetase family (ACSLs) represented by ACSL1, ACSL2, ACSL3, ACSL4, ACSL5 and ACSL6. Among them, ACSL4 plays a pivotal role in catalyzing the esterification of free PUFAs, which are subsequently incorporated into membrane phospholipids promoting lipid peroxidation-induced ferroptosis[20]. Dt significantly modulates the expression of all ACSLs genes, particularly by upregulating ACSL4 gene thus explaining the high level of membranes lipid oxidation displayed by MDAMB231 cells.

Several evidence indicate that transferrin receptor (TFR1) plays a crucial role in facilitating the entry of extracellular Fe^{3+} into the cell's endosomes, where it is reduced to Fe^{2+}, triggering ferroptosis[5]. Dt is also involved in this process with a role in the upregulation of TFR1 leading to increased iron intake, resulting in iron 'overload', lipid peroxidation and the onset of ferroptosis. Ferritin is responsible for iron storage in cells, through an intricate complex formed by two subunits, ferritin light polypeptide 1 (FTL1) and ferritin heavy polypeptide 1 (FTH1)[31]. Dt induces FTH1/FTL1 degradation through the overexpression of nuclear receptor coactivator 4 (NCOA4) and the activation of autophagy protein 5 (ATG5) and autophagy protein 7 (ATG7). This results in the releasing a substantial amount of free Fe^{2+} and elevating intracellular iron levels that in turn induces lipid peroxidation[32]. This hypothetic pathway is confirmed by a previous study reporting that autophagy related proteins ATG5 and ATG7 play a pivotal role in the degradation of ferritin, the reduction of iron reserves and the facilitation of ferroptosis processes[33]. Based on our results, a putative ferroptosis-like mechanism induced by Dt in the breast cancer MDAMB231 cells is suggested (Fig. 8). Dt increases intracellular Fe^{3+} intake with successive upregulation of the transferrin receptor. The reduction of Fe^{3+} to Fe^{2+} within cells is one of the key elements that promotes ferroptosis. Indeed, increasing levels of Fe^{2+} determines ROS production and recruits the GPX4/GSH machinery thus inhibiting antioxidant response and promoting lipid peroxidation through Fenton reaction (Fig. 8). Comparing with other studies[20,28,30], some of the targets such as GPX4, ACSL4, SLC7A11 are common and key-factors in ferroptosis mechanism. Therefore, they can be used as proxies in a bioprospecting studies seeking for natural compounds able to promote ferroptotic cell death.

The very low active concentration of Dt ($IC_{50} = 6$ ng ml^{-1}) as reported in this study is an important asset to claim the chemopreventive interest of this xanthophyll. Generally, it is known that marine natural compounds display greater bioactivity at lower concentration range (ppm to µMol) compared to compounds issued from terrestrial organisms[34,35]. For instance, pure molecules belonging to alkaloid family, isolated from sponges exhibited bioactivity with $IC_{50} = 12$ ppm[36].

The stability assessment unveils the resilience of Dt in vitro in biological fluids at 37 °C, both in culture medium and simulated body fluid. This is an important feature to further consider the use of Dt as potential

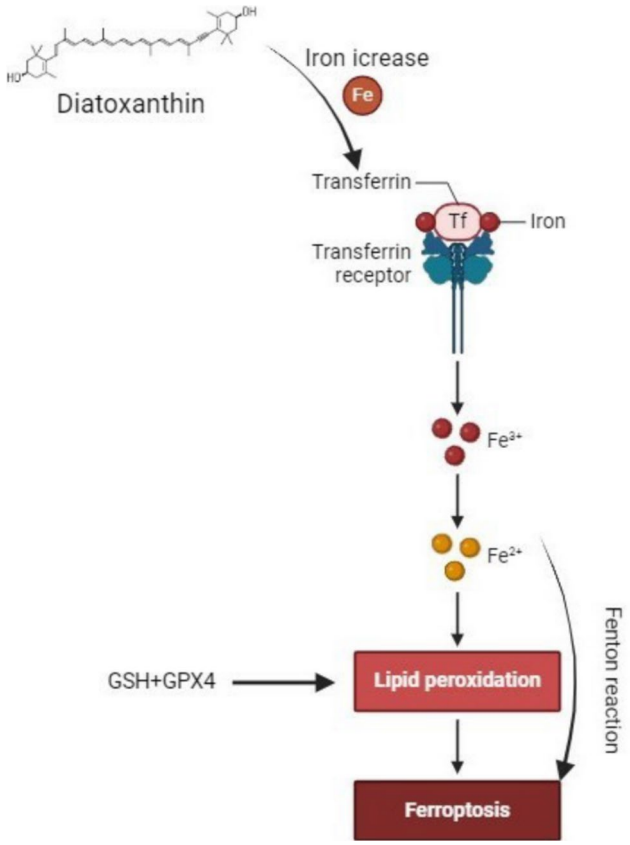

Fig. 8. Mechanism of action hypothesized for Dt on MDAMB231 cells.

therapeutic agent. It is noteworthy that Dt is significantly absorbed by MDAMB231 cells in 1 h, and almost totally assimilated in 3 h.

The half-life of Dt in human plasma has been estimated at around 25 min, which is in the mean of values reported for different synthetic drugs[37]. Propaedeutic to in vivo examination, the half-life of Dt in human plasma represents a crucial information[37] to acknowledge the potential development of Dt as chemopreventive agent. This information is also needed to design the best drug delivery strategy for Dt, such as for instance lipid nanoparticles as reported for ß-carotene[38]. Further validation of Dt interest as chemopreventive agent requires in vivo examination and clinical trials also to investigate the bio-accessibility of Dt—defined as the ratio of Dt solubilized in the mixed micelles *vs* the total Dt administered[39]. This is fully relied to the bioavailability of the molecules, such as Dt, which increases through their solubility in lipidic mixed micelle consisting of bile acids, phospholipids, cholesterol, fatty acids, and monoacylglycerols, allowing thus their accessibility to the intestinal epithelial cells[39].

Methods

Human cell lines

The triple negative breast cancer cell line (MDAMB231; ATCC number HTB-26, Manassas, VA, USA) and the breast adenocarcinoma cell line (MDAMB468; ATCC number HTB-132, Manassas, VA, USA) were grown in DMEM/F12 (1:1 mixture of DMEM medium and Ham′s F12 medium), supplemented with 2 mM L-Glut, 10% FBS and 100 units mL^{-1} penicillin and streptomycin (SLM-243-B, Sigma-Aldrich, St. Louis, MO, USA).

The three somatic cell lines were dermal fibroblasts (human neonatal dermal fibroblasts, ATCC number PCS-201-010, Manassas, VA, USA), HaCat (human keratinocytes, licensed and provided by Ceinge Institute, Naples) and melanocytes (Primary Epidermal Melanocytes; Normal, Human, Neonatal-HEMn, ATCC number, PCS-200-012, Manassas, VA, USA). Dermal fibroblasts were grown in fibroblast growth medium (116–500, Sigma-Aldrich, St. Louis, MO, USA). HaCat cells were cultivated in DMEM/F12 (1:1 mixture of DMEM medium and Ham′s F12 medium), supplemented with 2 mM L-Glut, 10% FBS and 100 units mL^{-1} penicillin and streptomycin (SLM-243-B, Sigma-Aldrich, St. Louis, MO, USA). The normal melanocytes were grown in melanocytes growth medium with supplements (C-24110, Sigma-Aldrich, St. Louis, MO, USA).

All the cell lines were cultured in a Forma™ Series II Water-Jacketed CO_2 Incubator (3111, Thermo Scientific, Waltham, MA, USA). Once cultures reached confluence (approximatively every 3 days), cells were detached by using trypsin and culture medium was changed. Before the experiments, cells were seeded in 6 or 96-well plates and kept overnight in thermostatic chamber in a 5% CO_2 atmosphere at 37 °C for the attachment.

Experimental design

Pure diatoxanthin (Dt) was purchased from D.H.I. Water & Environment (Hørsholm, Denmark). Five cell lines were used for cell viability assessment in presence or absence of Dt: MDAMB231, MDAMB468, dermal fibroblasts, HaCat, and melanocytes. For this analysis, the different cells were seeded in 96 well plate (transparent flat bottom, TPP Techno Plastic Products AG, Trasadingen, Switzerland), with an initial concentration of 2×10^3 cells $well^{-1}$ and kept overnight for attachment, in a thermostatic chamber in a 5% CO_2 atmosphere at 37 °C. After the attachment, each cell line was treated with twelve different concentrations of Dt i.e., 0.1, 0.5, 1, 1.5, 2, 2.5, 5, 7.5, 10, 12.5, 15 and 25 ng mL^{-1}.

For the following experiments, MDAMB231 cells were seeded in 6 well plate (transparent flat bottom, TPP Techno Plastic Products AG, Trasadingen, Switzerland), with an initial concentration of 2×10^6 cells $well^{-1}$ and kept overnight for attachment, in a thermostatic chamber in a 5% CO_2 atmosphere at 37 °C.

For the evaluation of the Dt effects on MDAMB231 cell line, cells were treated with Dt (6 ng mL^{-1}), as well as with erastin (ER, 10 µM; E7781, Sigma-Aldrich, St. Louis, MO, USA) and ferrostatin-1 (FS, 60 nM; SML0583, Sigma-Aldrich, St. Louis, MO, USA). Erastin is a well-known ferroptosis inducer and was considered as positive control, while ferrostatin-1, a well-known ferroptosis inhibitor, represented the negative control. Furthermore, we explored the effects of a combination between ferroptosis inducer and inhibitor, i.e., FS + Dt (FS + Dt, 60 nM and 6 ng mL^{-1}, respectively), and ER + FS (10 µM and 60 nM, respectively).

Viability test

For viability assays, diatoxanthin was suspended in ethanol (ETOH) at a final concentration of 1% (v/v). The cell viability was evaluated by 3-(4,5-Dimethylthiazol-2-yl)-2,5-Diphenyltetrazolium Bromide (MTT) assay (A2231, Applichem, Darmstadt, Germany) . The applied procedure was previously detailed[12]. After 48 h of treatment, 10 µL of MTT (5 mg mL^{-1}) were added to the cell medium and incubated in the dark for 3 h at 37 °C. Then, culture medium was aspirated and 100 µL of isopropanol were added for each well, incubating under agitation for 1 h to let the purple formazan crystals dissolving. The absorbance was recorded using a BioTek Synergy HTX Multimode Reader at a wavelength of 570 nm (Agilent, Santa Clara, CA, USA). The cytotoxic activity was measured as percentage of cell viability, obtained from the ratio between the mean absorbance of each sample and the mean absorbance of respective controls.

Western blot analysis

The following primary antibodies were used for wester: beta-actin (β-actin; 4970, Cell Signaling Technology Inc., Danvers, MA, USA), glutathione peroxidase 4 (GPX4; ab125066, Abcam, Cambridge, United Kingdom), transferrin receptor (TFRC; ab218544, Abcam, Cambridge, United Kingdom), ferritin heavy chain (FHC; ab183781, Abcam, Cambridge, United Kingdom). MDAMB231 were treated with ER (10 µM), FS (60 nM) or Dt (6 ng mL^{-1}). After 48 h of incubation, the medium was removed while the cell lysates were prepared by scraping each well into 500 µL of RIPA Lysis and Extraction Buffer (89,900, Thermo Fisher Scientific, Waltham, MA, USA), supplemented with Halt Protease & Phosphatase Inhibitor Cocktail (78,440, Thermo Fisher Scientific, Waltham, MA, USA). The lysate was incubated on ice for 15 min and then clarified by centrifugation at 14,000 × *g* for 20 min. Total protein concentration was determined according to the Bradford method using Bradford—Solution for Protein Determination (A6932, Applichem, Darmstadt, Germany), with bovine serum albumin (BSA, 1126GR100, neoFroxx, Einhausen, Germany) as a standard. The protein extracts were stored at − 20 °C until use. Before electrophoresis, protein samples were incubated at 95 °C for 5 min. Following, 10% SDS-PAGEs were stained with Coomassie Brilliant Blue R-250 Staining Solution (161–0436, Bio-Rad, Hercules, CA, USA) or blotted onto Trans-Blot Turbo Midi 0.2 µm Nitrocellulose membrane (170–4159, Bio-Rad, Hercules, CA, USA) using Trans-Blot Turbo Transfer System (170–4150, Bio-Rad, Hercules, CA, USA). Membranes were incubated for 1 h in blocking reagent (1X Tris Buffered Saline-TBS), with 0.1% Tween-20 with 5% *w*/*v* nonfat dry milk and incubated overnight at 4 °C with the primary antibodies diluted in 1X TBS, 0.1% Tween-20 with 5% BSA. GPX4 (antibody 1:10,000 diluted), TFRC (antibody 1:10,000 diluted) and FHC (antibody 1:10,000 diluted) proteins were investigated. Positive control was obtained by using an anti-β-Actin antibody (antibody 1:10,000 diluted). After incubation, membranes were washed three times for 10 min each with 15 mL of TBS/Tween and then incubated with Goat Anti-Rabbit IgG H&L (Alexa Fluor 488, antibody 1:500 diluted; ab150077, Abcam, Cambridge, UK) with gentle agitation for 1 h at room temperature. After incubation, membranes were washed three times for 5 min each with 15 mL of TBS/Tween. Blotted membranes were detected by visualizing proteins with ChemiDoc MP Imaging System (120–3154, Bio-Rad, Hercules, CA, USA). Densitometric analysis of immunopositive bands was performed using ImageLab software (Bio-Rad, Hercules, CA, USA).

Intracellular Fe^{2+} imaging

The imaging of intracellular Fe^{2+} was performed using Intracellular Iron Ion Measurement Kit—Ferrorange (F374, Dojindo, Kumamoto, Japan), following the manufacturer´s protocol. After 24 h of incubation with Dt (6 ng mL^{-1}), cells were washed three times with 200 µL of Hanks' Balanced Salt Solution (HBSS, 88,284, Thermo Fisher Scientific, Waltham, MA, USA) and then 200 µL of HBSS solution containing FerroOrange (1 µmol L^{-1}) and 2,2'-bipyridyl (Bpy, 100 µmol L^{-1}) were added to the cells. Cells were incubated for 30 min in a 37 °C incubator equilibrated with 95% air and 5% CO_2, and then observed under an Epifluorescence microscope (Axioscope, Carl Zeiss, Oberkochen, Germany).

Glutathione and glutathione synthetase quantification assay

For the glutathione quantification, after 24 h of incubation with Dt (6 ng mL^{-1}), MDAMB231 cells were harvested by using trypsin. After harvesting, cells were washed with 300 µL of Phosphate Buffer Saline (PBS) and centrifuged at 200 × *g* for 10 min at 4 °C to remove the supernatant. For the lysis of the cells, 80 µL of 10 mmol

L^{-1} were added and two freezing/thawing cycles were performed. Finally, 20 µL of 5% 5-Sulfosalicylic acid (SSA) solution was added and the cell suspension was then centrifuged at 800 × *g* for 10 min. After centrifugation, the supernatant was transferred into fresh tubes and the solution was diluted in ddH_2O, aiming to dilute the SSA to the final concentration (0.5%). The samples obtained were then used for the quantification of glutathione by using the GSSG/GSH quantification kit (G257, Dojindo, Kumamoto, Japan), following to the manufacturer's protocol.

Lipid peroxide detection

For the detection of lipid peroxide cells were incubated for 1, 3 and 24 h with five different treatments i.e., Dt (6 ng mL^{-1}), ER (10 µM), FS (60 mM), FS + Dt (60 mM and 6 ng mL^{-1}, respectively) and ER + FS (10 µM and 60 mM, respectively). After incubation, the supernatant was removed and the cells were washed with HBSS. After washing, the detection of lipid peroxide was performed by using the Liperfluo kit (L248, Dojindo, Kumamoto, Japan) according to the manufacturer´s protocol. At the end of the protocol, cells were then harvested by trypsinization and collected into a microtube with culture medium. The supernatant was replaced with HBSS, and cells were analyzed using BD Accuri C6 Plus Flow Cytometer FACS (BD Bioscience, Heidelberg, Germany; Excitation: 488 nm, Emission: 500–550 nm).

RNA extraction and gene expression analysis

For gene expression studies, cells were incubated for 1, 3 and 24 h with five different treatments i.e., Dt (6 ng mL^{-1}), ER (10 µM), FS (60 mM), FS + Dt (60 mM and 6 ng mL^{-1}, respectively) and ER + FS (10 µM and 60 mM, respectively). At the end of the treatment, cells were washed by adding cold Phosphate Buffered Saline (PBS) and then lysed directly in plates by adding 1 mL of TRIsure reagent (BIO-3803, Meridian Bioscience Inc., Cincinnati, OH, USA) and RNA was isolated according to manufacturer's protocol. RNA concentration (expressed as ng μL^{-1}) and purity (evaluating A260/A280 and A260/A230 ratios) were assessed using the NanoDrop 1000 Spectrophotometer (Thermo Fisher Scientific, Waltham, MA, USA), estimating the volume of RNA solution necessary to obtain 200 ng of cDNA by reverse transcription. The reverse transcription reaction was carried out qScript cDNA SuperMix (95,048, QuantaBio, Beverly, MA, USA), according to manufacturer's protocol. Primers' design (**see** Table S1) and validation were performed for the assessment of RT-qPCR experiments.

RT-qPCR experiments were performed in triplicates by using a RT^2 SYBR Green qPCR Mastermix (330,502, Qiagen, Hilden, Germany)) in 384 well plates and were run on a ViiA7 (Applied Biosystems, Waltham, MA, USA) through Standard Fast PCR Cycling protocol with 10 µL of final reaction. Temperature program was set as follows: i) 1 cycle at 95 °C for 10 min and ii) 40 amplification cycles at 95 °C for 15 s and 60 °C for 1 min. Amplification data were collected by using a ViiA 7 Software (Applied Biosystems, Waltham, MA, USA). The cycle threshold (Ct)-values were then analysed through PCR array data analysis available online software (https://dataanalysis2.qiagen.com/pcr, Qiagen, Hilden, Germany). A quality check control, evaluating possible genomic DNA contamination, reverse transcription efficiency and PCR array reproducibility, was done. Fold change values (gene expression ratios) were calculated based on the 2(-ΔΔCt) method[33]. Control genes used for data normalization were actin-beta (ACTB), beta-2-microglobulin (B2M), glyceraldehyde-3-phosphate dehydrogenase (GAPDH), Hypoxanthine phosphoribosyltransferase 1 (HPRT1) and ribosomal protein, large subunit P0 (RPLP0), whose expression was found unchanged in control and treated cells. To show a more readable gene expression data, fold changes (x) were converted to fold regulation values as $\left(-\frac{1}{x}\right)$. Cut-off was set at ± 2.

Diatoxanthin analysis by HPLC

To retrieve the Dt concentration in the different fluids, HPLC was used. Dt analysis was done following the protocol[40] in a HPLC Hewlett Packard series 1100, equipped.

with a reversed-phase column (2.6 mm diameter C8 Kinetex column; 50 × 4.6 mm.; Phenomenex,

Torrance, CA, USA). Determination and quantification of Dt was carried out using pigment standards from the D.H.I. Water and Environment (Danish Hydraulic Institute; Horsholm, Denmark).

Diatoxanthin in vitro stability assessment

Cell culture medium

The in vitro stability of Dt was investigated in MDAMB231 culture medium (DMEM/F12 supplemented with 10% of FBS) with or without cells. Dt was added to the culture medium at a final concentration of 6 ng mL^{-1}. The assays were performed in a shaking thermostatic chamber at 37 °C and performed in triplicate. Samples were collected at 0, 1, 3 and 24 h, and the culture medium was filtered onto 0.2 µm filter before injection into the HPLC (see before).

Simulated body fluid (SBF)

The in vitro stability of Dt was studied in a simulated body fluid (SBF) prepared according to Ref.[41] and modified[42].

Dt was added to SBF at a final concentration of 6 ng mL^{-1}. The assays were performed in a shaking thermostatic chamber at 37 °C and performed in triplicate. Samples were collected at 0, 1, 3 and 24 h. The simulated body fluid was filtered onto 0.2 µm filter before injection into the HPLC (see before).

Human plasma

The in vitro stability of Dt was studied in human plasma following the protocol[38]. Plasma from human was supplied by Sigma Chemical Company (St. Louis, MO, USA). The plasma was diluted to 80% with 0.05 M PBS (pH 7.4) at 37°C.

Dt was added to 500 µL of pre-heated plasma solution at a final concentration of 6 ng mL^{-1}. The assays were performed in a shaking thermostatic chamber at 37 °C and performed in triplicate. Samples (500 µL) were collected at 0, 15, 30, 45, 60, 90 min and added to 2 mL acetonitrile to deproteinize the plasma. The samples were then mixed by vortexing for 1 min and centrifuged at 4 °C for 15 min at 14,000 rpm. The clear supernatants were analyzed by HPLC, after filtration onto 0.2 µm filter.

The in vitro plasma half-life ($t_{1/2}$) was calculated using the expression $t_{1/2} = 0.693/b$, where b.

is the slope found in the linear fit of the natural logarithm of the fraction remaining of the parent compound vs. incubation time[38].

Data availability

The dataset used and analyzed during this current study is available from the corresponding author on reasonable request.

Received: 7 June 2024; Accepted: 20 February 2025
Published online: 09 March 2025

References

1. National Cancer Institute. *Cancer Stat Facts: Female Breast Cancer*. https://seer.cancer.gov/statfacts/html/breast.html (2024).
2. Aysola, K. et al. Triple negative breast cancer - An Overview. *Hered. Genet.* **2013**(Suppl 2), 001 (2013).
3. Chen, Z. et al. Ferroptosis as a potential target for cancer therapy. *Cell Death Dis.* **14**, 460 (2023).
4. Koren, E. & Fuchs, Y. Modes of regulated cell death in cancer. *Cancer Discov.* **11**, 245–265 (2021).
5. Sui, S. et al. Ferritinophagy is required for the induction of ferroptosis by the bromodomain protein BRD4 inhibitor (+)-JQ1 in cancer cells. *Cell Death Dis.* **10**, 331 (2019).
6. Liu, Y., Hu, Y., Jiang, Y., Bu, J. & Gu, X. Targeting ferroptosis, the achilles' heel of breast cancer: a review. *Front. Pharmacol.* **13**, 1036140 (2022).
7. Jiang, X. P., Elliott, R. L. & Head, J. F. Manipulation of iron transporter genes results in the suppression of human and mouse mammary adenocarcinomas. *Anticancer Res.* **30**, 759–765 (2010).
8. Hou, C. et al. Serum iron status and the risk of breast cancer in the European population: a two-sample Mendelian randomisation study. *Genes Nutr.* **16**, 9 (2021).
9. Lee, S., Jeon, H. & Shim, B. Prognostic value of ferritin-to-hemoglobin ratio in patients with advanced non-small-cell lung cancer. *J. Cancer* **10**, 1717–1725 (2019).
10. Ge, A. et al. Mechanism of ferroptosis in breast cancer and research progress of natural compounds regulating ferroptosis. *J Cell Mol. Med.* **28**, e18044 (2024).
11. Andrijauskaite, K. & Wargovich, M. J. Role of natural products in breast cancer related symptomology: targeting chronic inflammation. *Semin. Cancer Biol.* **80**, 370–378 (2022).
12. Sansone, C. et al. The carotenoid diatoxanthin modulates inflammatory and angiogenesis pathways in vitro in prostate cancer cells. *Antioxidants (Basel)* **12**, 359 (2023).
13. Smerilli, A. et al. Photoprotective and antioxidant responses to light spectrum and intensity variations on a coastal diatom. *Environ. Microbiol.* **19**, 611–627 (2017).
14. Brunet, C. et al. Measured photophysiological parameters used as tools to estimate vertical water movements in the coastal Mediterranean. *J. Plankton Res.* **25**, 1413–1425 (2003).
15. Beer, A., Juhas, M. & Büchel, C. Influence of different light intensities and different iron nutrition on the photosynthetic apparatus in the diatom *Cyclotella meneghiniana* (Bacillariophyceae) (1). *J. Phycol.* **47**, 1266–1273 (2011).
16. Noonan, D. M. *et al.* The algal carotenoid diatoxanthin shows anti-cancer and cardio-protective properties: RNA seq analysis of potential targets [abstract]. In: Proc. of the American Association for Cancer Research Annual Meeting 2024; Part 1 (Regular Abstracts); 2024 Apr 5–10; San Diego, CA. Philadelphia (PA): AACR; Cancer Res 2024;84(6_Suppl): Abstract nr 7303 (2024).
17. Chavez, K. J., Garimella, S. V. & Lipkowitz, S. Triple negative breast cancer cell lines: one tool in the search for better treatment of triple negative breast cancer. *Breast Dis.* **32**, 35–48 (2010).
18. Li, Z. et al. Targeting ferroptosis in breast cancer. *Biomark. Res.* **8**, 58 (2020).
19. Stockwell, B. R. Ferroptosis turns 10: emerging mechanisms, physiological functions, and therapeutic applications. *Cell* **185**, 2401–2421 (2022).
20. Doll, S. et al. ACSL4 dictates ferroptosis sensitivity by shaping cellular lipid composition. *Nat. Chem. Biol.* **13**, 91–98 (2017).
21. Zhao, L. et al. Ferroptosis in cancer and cancer immunotherapy. *Cancer Commun. (Lond.)* **42**, 88–116 (2022).
22. Wang, Z. et al. Dihydroartemisinin triggers ferroptosis in primary liver cancer cells by promoting and unfolded protein response-induced upregulation of CHAC1 expression. *Oncol. Rep.* **46**, 240 (2021).
23. Chen, M.-S. et al. CHAC1 degradation of glutathione enhances cystine-starvation-induced necroptosis and ferroptosis in human triple negative breast cancer cells via the GCN2-eIF2α-ATF4 pathway. *Oncotarget* **8**, 114588–114602 (2017).
24. Wen, Y. et al. Glycyrrhetinic acid induces oxidative/nitrative stress and drives ferroptosis through activating NADPH oxidases and iNOS, and depriving glutathione in triple-negative breast cancer cells. *Free Radic. Biol. Med.* **173**, 41–51 (2021).
25. Ding, Y. et al. Identification of a small molecule as inducer of ferroptosis and apoptosis through ubiquitination of GPX4 in triple negative breast cancer cells. *J. Hematol. Oncol.* **14**, 19 (2021).
26. Pistelli, L. et al. MMP-9 and IL-1β as targets for diatoxanthin and related microalgal pigments: potential chemopreventive and photoprotective agents. *Mar Drugs* **19**, 354 (2021).
27. Brunet, C., Casotti, R., Aronne, B. & Vantrepotte, V. Measured photophysiological parameters used as tools to estimate vertical water movements in the coastal Mediterranean. *J. Plankton Res.* **25**, 1413–1425 (2003).
28. Huang, C. et al. Upregulation and activation of p53 by erastin induced reactive oxygen species contribute to cytotoxic and cytostatic effects in A549 lung cancer cells. *Oncol. Rep.* **40**, 2363–2370 (2018).
29. Jiang, L. et al. Ferroptosis as a p53-mediated activity during tumour suppression. *Nature* **520**, 57–62 (2015).
30. Park, T.-J. et al. Quantitative proteomic analyses reveal that GPX4 downregulation during myocardial infarction contributes to ferroptosis in cardiomyocytes. *Cell Death Dis.* **10**, 835 (2019).
31. Manz, D. H., Blanchette, N. L., Paul, B. T., Torti, F. M. & Torti, S. V. Iron and cancer: recent insights. *Ann. N. Y. Acad. Sci.* **1368**, 149–161 (2016).
32. Hou, W. et al. Autophagy promotes ferroptosis by degradation of ferritin. *Autophagy* **12**, 1425–1428 (2016).

33. Livak, K. J. & Schmittgen, T. D. Analysis of relative gene expression data using real-time quantitative PCR and the 2(-Delta Delta C(T)) Method. *Methods* **25**, 402–408 (2021).
34. Montaser, R. & Luesch, H. Marine natural products: a new wave of drugs?. *Future Med. Chem.* **3**, 1475–1489 (2011).
35. Carroll, A., Copp, B., Davis, R., Keyzers, R. & Prinsep, M. Marine natural products. *Nat. Prod. Rep.* **36**, 122–173 (2019).
36. Bashari, M. H. et al. The ethanol extract of marine sponge *Aaptos suberitoides* suppress cell viability, cell proliferation and cell migration in HER2-positive breast cancer cell line. *Asian Pac. J. Cancer Prev.* **22**, 25–32 (2021).
37. Konsoula, R. & Jung, M. *In Vitro Plasma* Stability, Permeability and Solubility of Mercaptoacetamide Histone Deacetylase Inhibitors. *Int. J. Pharm.* **361**, 19–25 (2008).
38. Mahmood, Q. et al. Targeted delivery of β-carotene potentially prevents blood-brain barrier breakdown after stroke in mice. *Phytomed. Plus* **3**, 100426 (2023).
39. Kotake-Nara, E. & Nagao, A. Absorption and metabolism of xanthophylls. *Mar. Drugs* **9**, 1024–1037 (2011).
40. Manfellotto, F. et al. Engineering the unicellular alga *Phaeodactylum tricornutum* for enhancing carotenoid production. *Antioxidants* **9**, 757 (2020).
41. Kokubo, T. Surface chemistry of bioactive glass-ceramics. *J. Non Cryst. Solids* **120**, 138–151 (1990).
42. Jalota, S., Bhaduri, S. B. & Tas, A. C. Using a synthetic body fluid (SBF) solution of 27 mM HCO_3^- to make bone substitutes more osteointegrative. *Mater. Sci. Eng. C Mater. Biol. Appl.* **28**, 129–140 (2008).

Acknowledgements

Luigi Pistelli has been supported by a PhD fellowship funded by the Stazione Zoologica Anton Dohrn. Research has been partly funded by the "SCANFISH: SEA COSMETICS & NUTRACEUTICS: FROM FISHERY & AQUACULTUREBYPRODUCTS" project (funded by CNR, CUP: B67G22000150005).

Author contributions

C.S. and C.B. conceived the research. C.S. and L.P. designed the experiments and performed the data analysis. All authors discussed the data and wrote the paper. All authors contributed and revised the manuscript.

Declarations

Competing interests

The authors declare no competing interests.

Additional information

Supplementary Information The online version contains supplementary material available at https://doi.org/10.1038/s41598-025-91519-6.

Correspondence and requests for materials should be addressed to C.S.

Reprints and permissions information is available at www.nature.com/reprints.

Publisher's note Springer Nature remains neutral with regard to jurisdictional claims in published maps and institutional affiliations.